Spoof surface plasmon resonant tunneling mode with high quality and Purcell factors

Soumitra Roy Joy, Mikhail Erementchouk, and Pinaki Mazumder

Phys. Rev. B **95**, 075435 — Published 28 February 2017

DOI: 10.1103/PhysRevB.95.075435

Spoof Surface Plasmon Resonant Tunneling Mode with High Quality and Purcell Factor

Soumitra Roy Joy,* Mikhail Erementchouk,† and Pinaki Mazumder‡

Department of Electrical Engineering and Computer Science,

University of Michigan, Ann Arbor, MI 48109 USA

Abstract

High quality factor and small modal volume for compact, integrable optical devices have always been of great demand. Although metamaterials may be designed to achieve selected mode confinement at a subwavelength scale, structures themselves have retained a large size. We address the issue of the subwavelength mode confinement in structures of reduced size by utilizing unique properties of spoof surface plasmon polaritons (SSPP). While SSPP modes are commonly considered in the context of periodic structures, we demonstrate that the SSPP formation does not depend crucially on periodicity and, therefore, meta-structures of minimal length can support well-formed spoof plasmon state. This general property is explicated through our study of the transmission spectrum of a three-cell waveguide with the spoof plasma frequency of the middle cell (defect cell) different from that of remaining cells (host). The SSPP state in the defect cell supports resonant tunneling manifested by a narrow transmission resonance inside the bandgap of the host structure. Despite the minimal length of the structure, the localized defect SSPP mode is characterized by very high quality ($\sim 10^5$) and Purcell ($\sim 10^3$) factors. The proposed concept can be a promising alternative for making a miniaturized sources, information storage and sensing devices at low terahertz frequencies.

I. INTRODUCTION

The idea of spoof surface plasmon in a perforated metallic structure triggered by Pendry with coworkers[1] ushered in a great deal of work in this field that ramified into spoof versions of surface plasmon polariton[2–8] and localized surface plasmon[9–11] in subsequent years. The concept of spoof plasmon quasi-particle provides a way to adopt plasmonics to a lower frequency region where no true plasmons can exist because of high conductivity of metals. A patterned metal surface, however, can support a surface bound mode mimicking a surface plasmon mode without penetrating into the material[12]. It can be shown that the macroscopic behavior of the patterned metal surface demonstrates characteristic Drude model dispersion[1,13,14] with the spoof plasma frequency determined by the geometry of corrugations. To explain the working principle of spoof surface plasmon polartions (SSPP), several theories[13,15] describe SSPP structures, a specific type of meta-materials consisting of narrow grooves with sub-wavelength width on a plain metal surface [see Fig. 1(a)], in terms of an effective homogeneous medium. It is a commonly held belief that an effective medium description of a meta-structure breaks down as the number of elementary cells becomes too small[16]. In contrast to this argument, we show here that SSPP structures can preserve the same 'effective medium' description even when the size of the structure is reduced down to minimal number of unit cells. This facilitates building a very short and geometrically simple 1D SSPP structure, which is able to manifest excellent mode confinement quality yielding high Q-factor ($\sim Q_{max} \approx 10^5$) and high Purcell factor $\sim 10^3$. Spoof plasmon states defined by their dispersion relation are well preserved in finite structures, as periodicity plays a nominal role in determining its propagation character, which is in strong contrast to photonic crystal structures[17] in general.

Pre-engineered defects in plasmonic[18,19] and photonic structures[20] attract a great deal of scientific and engineering interest. Sophisticated applications such as ultra-small filters, low threshold lasers[21,22], photonic chips, multiplex biosensing[23] and quantum information processing[24,25] often seek for a structure supporting modes with high quality factor, Q, and small modal volume, V. For example, a point defect embedded into a large photonic crystal can yield a high-Q resonant mode inside the photonic bandgap. However, many applications require devices with stringent conditions of small sizes. In those cases, diffraction based devices, e.g., photonic-crystals, are disadvantageous since their feature size (i.e., lattice

parameter) has to be comparable to wavelength. Meta-materials, with their ability to offer deep subwavelength confinement[26,27], stand out to be better candidates for small devices. Efforts for making a small cavity size of good quality have so far resorted to embed the defect into a large array of unit cells with the number of cells reaching an order of 10^2 or even higher[28–30]. The large size of optical structures is apparently inevitable due to the following. Defect states form inside the bandgap of host medium. In both photonic crystals or metamaterials, the optical bandgap of the host structure is formed as a result of interference of multiple scattered waves. Therefore, one has to leave a significant amount of unit cells around the defect in order to faithfully reproduce the effect of periodic structure. A similar bandgap effect is observed in disordered metamaterials, which also involve a large ($\approx 10^2$) number of unit cells to embed a defect[31]. High quality mode proposed or realized by far, thus, inexorably bring large structures.

Our observations of the properties of an SSPP waveguide reveals a staggering fact. The characteristic transmission properties of SSPP modes obliterate the need for a long structure. This can enable to realize a high-Q resonant tunneling of spoof plasmon mode in a very short host medium. We illustrate this observation by considering a chain of three unit cells of a SSPP waveguide, with the first and last grooves having height h_h, and the groove at the middle having height h_d. We show that, for $h_d \neq h_h$, a resonant tunneling mode inside the SSPP bandgap is formed. Thus, we can reduce the entire structure of 'a defect in a host' system to its minimal possible length. In the subsequent sections, we will refer to this minimal length 'host-defect-host' heterogeneous system as a (1–1–1) structure.

II. TRANSMISSION SPECTRA OF HOMOGENEOUS AND HETEROGENEOUS STRUCTURES

A schematic of the structure under study is presented in Fig. 1(a). Periodic structures were a subject of intensive research[32–35] and their basic properties are well established. The SSPP dispersion diagram in a periodic structure is presented in Fig. 1(b). The gaps in the spectrum indicate the frequency regions where finite SSPP structures demonstrate subsided transmission as is illustrated by spectra shown in Fig. 2(a). The transmission coefficient of the waveguide stays close to unity in a wide frequency range with slight modulation by Fabry-Perot ripples and is strongly reduced in the bandgap zone.

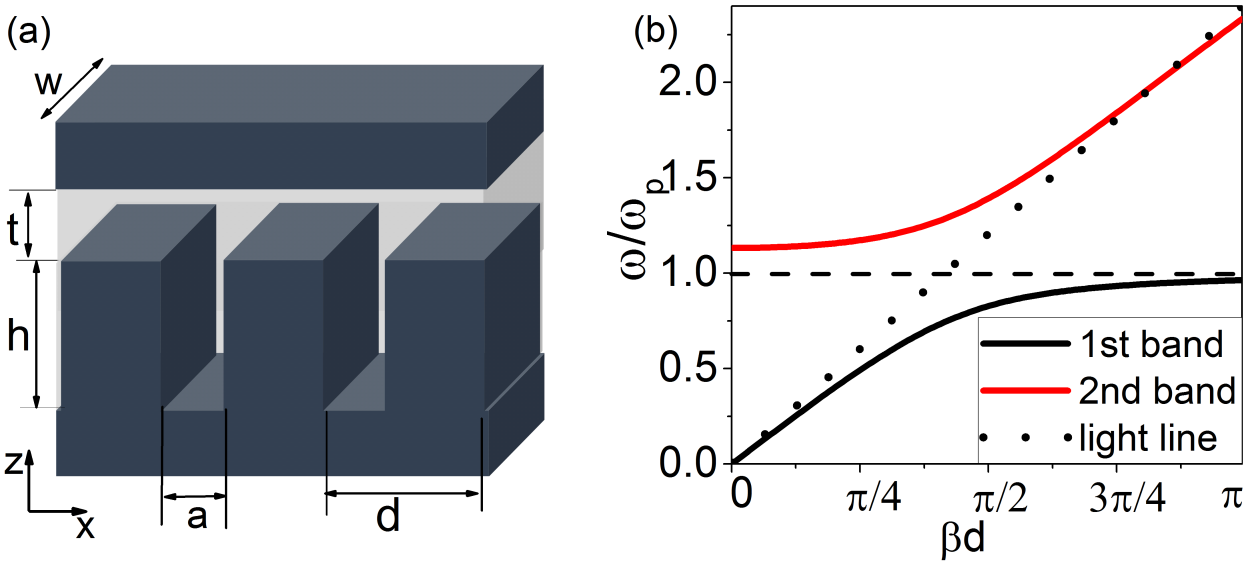

FIG. 1. (a) The geometry of a homogeneous SSPP structure. The dark regions indicate metal and the light regions correspond to dielectric. (b) The dispersion diagram of a periodic SSPP waveguide with $h/d \sim 1$, $t/d \sim 0.3$, $a/d \sim 0.1$, and $w \sim \lambda$. The frequency is normalized by the spoof plasma frequency $\omega_p = \pi c/2h$. The bandgaps are formed due to anti-crossing between light-line and ω_p. For $2h \gg d$, the anti-crossing happens far away from the Brillouin zone boundary.

A thorough treatment of the optical response of a good conductor's surface with periodic narrow grooves shows[14] that such structures are characterized by an effective Drude model with a spoof plasma frequency

$$\omega_p = \frac{\pi c}{2h\sqrt{\epsilon}}, \tag{1}$$

where h is the height of the grooves, c is the speed of light in vacuum and ϵ is the dielectric function of the medium filling the groove. It should be emphasized that this frequency does not derive from material properties, but from the geometry of the structure. Generally, taking into account higher order resonances, the n-th spoof plasma frequency can be written as

$$\omega_p^{(n)} = (2n-1)\omega_p, \tag{2}$$

with $n = 1, 2 \ldots$.

Figure 2(a) shows that major characteristics of transmission spectra of an SSPP waveguide successfully retain when the number of unit cells is greatly reduced. This result implies a certain immunity of SSPP modes to finite-size effects. Manifestation of strongly attenuated

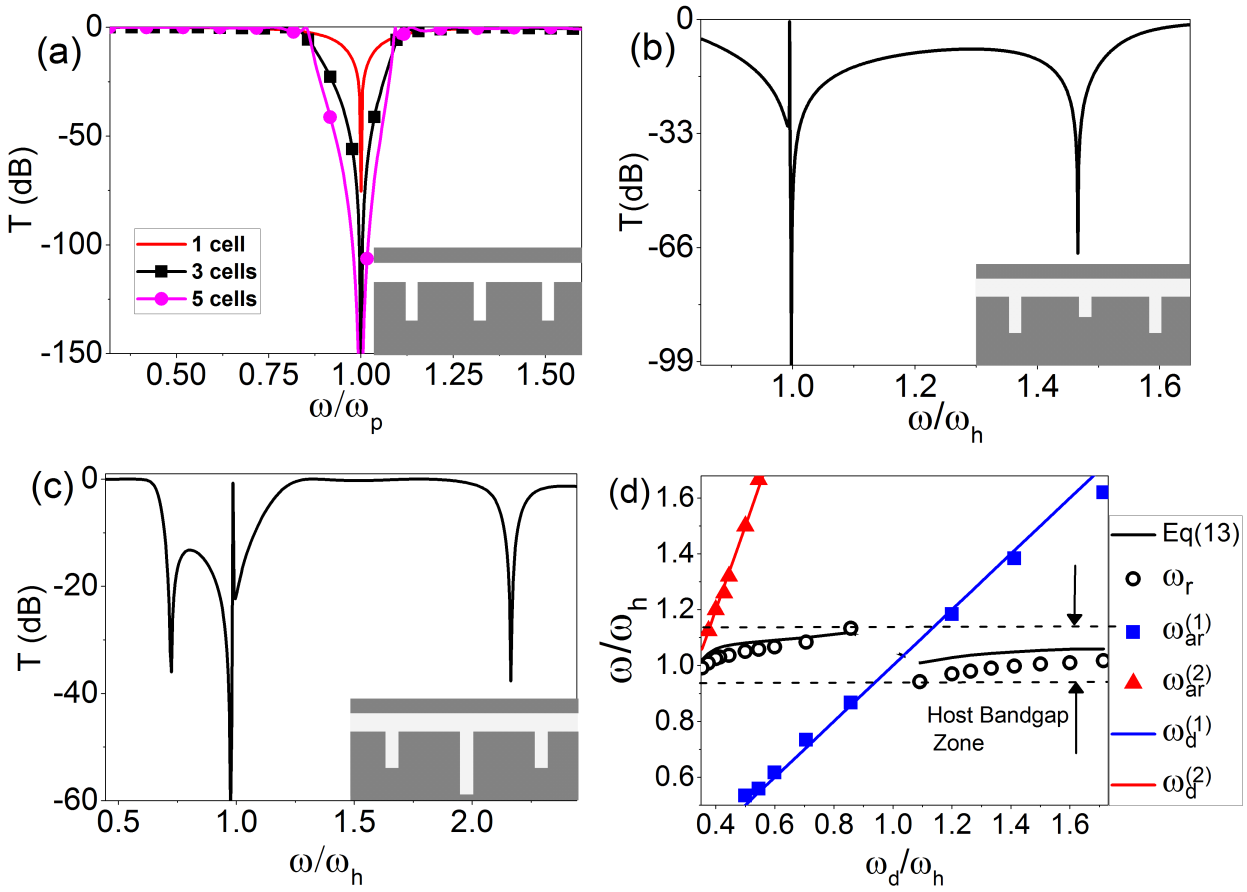

FIG. 2. (a) Transmission spectra of homogeneous SSPP waveguides with different number of unit cells. Inset shows the corresponding SSPP structure. (b,c) Transmission spectra of heterogeneous structures with the defect cells characterized by $h_d/h_h = 0.75$ and $h_d/h_h = 1.25$, respectively. Anti-resonances $\omega_{ar}^{(1)}$ and $\omega_{ar}^{(2)}$ (transmission dips) at $\omega/\omega_h \neq 1$ are induced by first and higher order spoof plasmon resonance modes of defect cells $\omega_d^{(1)}$ and $\omega_d^{(2)}$, respectively. In addition, a transmission resonance ω_r emerges inside the bandgap. The insets show corresponding heterogeneous geometry. (d) Trajectories of ω_r, $\omega_{ar}^{(1)}$ and $\omega_{ar}^{(2)}$ in heterogeneous SSPP structures as functions of the spoof plasma frequency of the defect cell. The solid black curves shown inside host bandgap are loci of ω_r obtained via Eq. (13). The dots of ω_r and $\omega_{ar}^{(n)}$ are the numerical data of the loci of the resonance and the n-th antiresonance, respectively, obtained from COMSOL Multiphysics simulation. Note that, the locus of transmission resonances ω_r demonstrates discontinuity around $\omega_d/\omega_h \sim 1$, as at this condition, the SSPP structure becomes homogeneous and contains no resonance inside bandgap.

transmission or anti-resonance of a single cell is utilized to propose spectral filters in several works[36,37], albeit in a different context. The attenuated transmission near an embedded cavity resonance is a characteristic feature of a laterally coupled waveguide-cavity systems in general[38]. In the present work, however, we emphasize that a single cell of spoof plasmon waveguide yields not only the 'bandgap effect' but also the 'dispersion effect' of a periodic structure. The 'bandgasp effect' refers to the phenomenon of strongly attenuated transmission in a finite SSPP waveguide over a frequency range that corresponds to the bandgap of its infinite version. The 'dispersion effect' in the context of finite structures should be understood in terms of a phase relation between the states of the field at the boundaries of a unit cell at a given frequency as is explicated in the transfer matrix treatment in section III.

To demonstrate these phenomena, we study the transmission behavior of a composite (1–1–1) structure of SSPP waveguide. We will call the middle cell a 'defect' with the groove height $h_d \neq h_h$ embedded in a host medium. The term 'defect' in this context means an intentional breaking of translation symmetry of an otherwise regular structure. As we will show, the transmission property of the composite medium can be successfully explained by considering each cell as an effective individual SSPP medium, characterized by ω_h and ω_d spoof plasma frequencies, respectively. To put differently, the effective medium description of a SSPP meta-structure is valid for a single cell as well. This simple concept has far greater significance than being of a mere theoretical interest. This helps in designing, as we will show, a very short spoof plasmon structure with giant quality and Purcell factors.

The transmission spectrum of the composite structure is a result of interplay between characteristic frequencies describing states of the field in periodic structures. A straightforward impact of inclusion of a new cell to an SSPP waveguide is added spectral filtering effect due to the SSPP bandgap, which manifests as an anti-resonance in the transmission spectrum [Fig. 2(b,c)]. The spatial distribution of the electric field inside the structure corresponding to different propagation regimes is shown in Fig. 3.

In addition to spectral filtering, the spectrum of an 1-1-1 structure may demonstrate a non-trivial phenomenon of transmission resonance due to resonant tunneling at frequencies inside the host SSPP bandgap [see Fig. 2(b,c)]. The characteristic field distribution in the resonant tunneling mode is shown in Fig. 3(c). Figure 2(d) depicts the trajectories of the transmission resonances ω_r and anti-resonances ω_{ar} with variation of ω_d. In the next section,

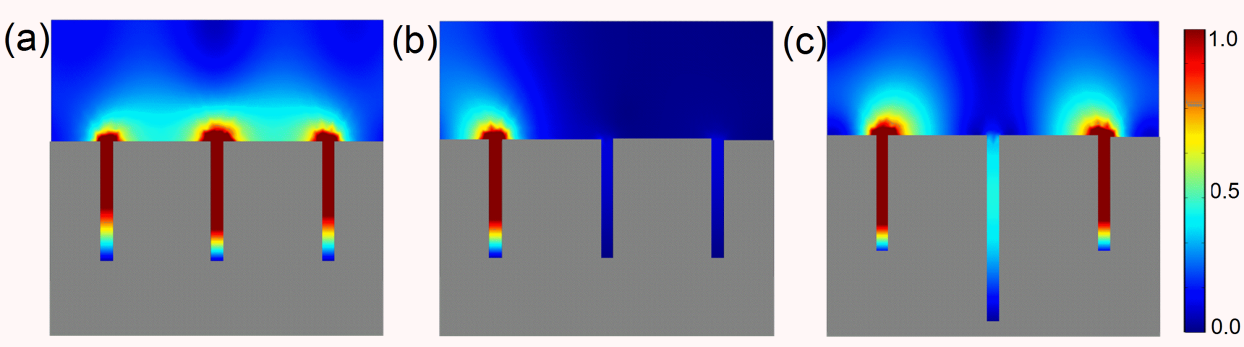

FIG. 3. Spatial field distribution inside a three-cell structure with the wave incident from the left side. (a) A propagating SSPP mode in a homogeneous structure at a frequency corresponding to a pass-band. (b) SSPP attenuation at a frequency inside a bandgap. (c) Resonant tunneling in a heterostructure incorporating a defect cell in the middle.

we show how the numerically obtained trajectory of ω_r and ω_{ar} in a (1–1–1) composite structure can be explained by describing the propagating state in each single cell as a spoof plasmon mode. In this regard, it should be emphasized that, as Fig. 3 demonstrates, all modes, propagating, non-propagating and resonant tunneling, are concentrated close to the surface of the structure. Appearance of such kind of resonant tunneling mode of spoof plasmon with high Q-factor in short structures is the principle message of the present work.

III. SSPP SCATTERING IN HETEROGENEOUS STRUCTURES

Despite significant efforts invested into theoretical studies of SSPP, a full yet tractable description of the propagation of spoof plasmons in finite structures is yet to be developed. Basic transport properties of such structures, however, can be understood using a simplified model based, first, on the assumption that the propagation within a single cell can be effectively characterized by an SSPP dispersion law and, second, on continuity-on-average conditions imposed at the interfaces between different cells.

In what follows, we will denote host and defect cells with subscripts 'h' and 'd', respectively. Retaining a single mode, the electric and magnetic fields can be presented as

$$H_y = e^{iq(\omega)z}\{f_+ e^{i\beta(\omega)x} + f_- e^{-i\beta(\omega)x}\} \tag{3}$$

$$E_z = -\frac{\beta(\omega)}{\omega\epsilon} e^{iq(\omega)z}\{f_+ e^{i\beta(\omega)x} - f_- e^{-i\beta(\omega)x}\}, \tag{4}$$

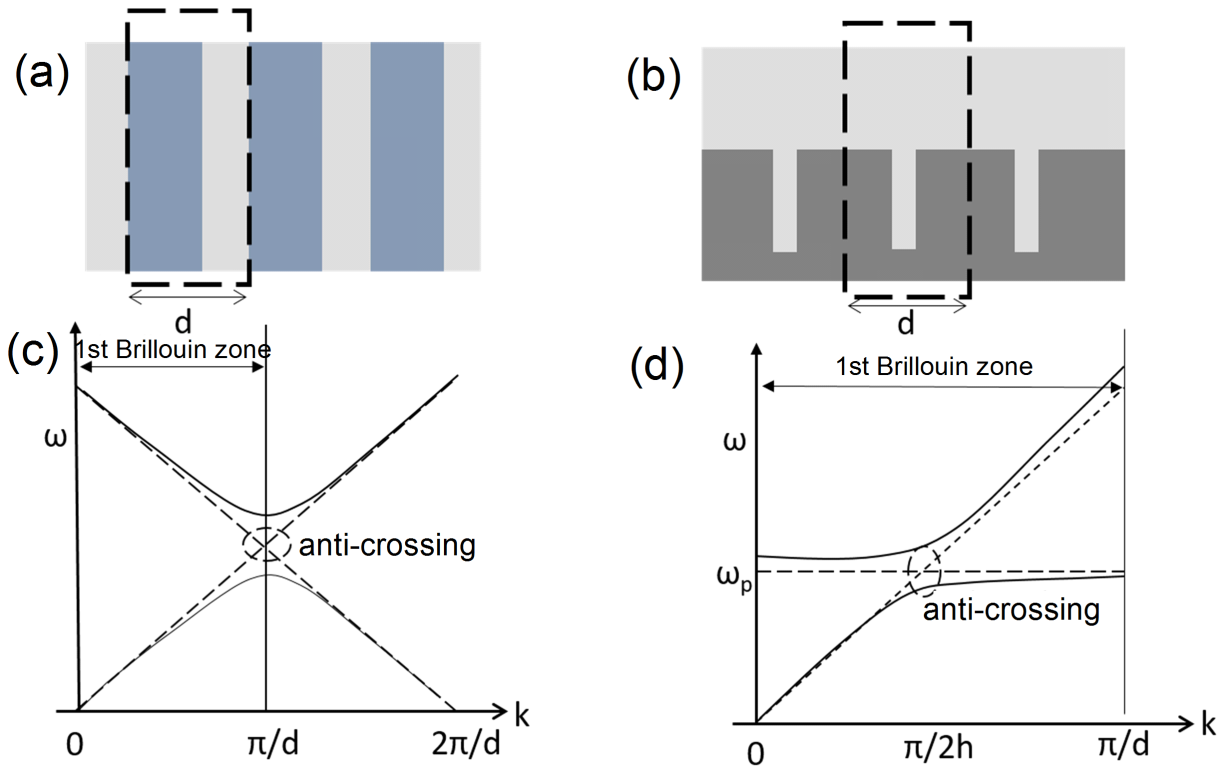

FIG. 4. (a,b) A 1D photonic crystal and an SSPP structure, respectively. The dashed box indicates the unit cell. (c,d) Band diagrams of a photonic crystal and a SSPP periodic waveguide, respectively. Anti-crossing (dashed circles) between bands of the perturbed background (dashed lines) leads to formation of new bands (solid lines). For the SSPP, the anti-crossing location ($k = \pi/2h$) must occur far away from the boundary of the Brillouin zone in order to have well developed SSPP. As a result, SSPP modes are immune to broken periodicity and withstand the finite size effect.

where the coordinate axes are chosen as shown in Fig. 1(a), f_+ and f_- are amplitudes of the waves propagating forward and backward, respectively, $q(\omega) = \sqrt{(\omega/c)^2 - \beta^2(\omega)}$ is the transverse wavenumber and $\beta(\omega)$ is found for the host and defect cells from the respective dispersion equations $D_{h,d}(\omega, \beta) = 0$, where[39]

$$D(\omega, \beta) = \frac{q}{\omega/c}\tan(qt) + \frac{a}{d}\mathrm{sinc}^2(a\beta/2)\tan(\omega h/c), \tag{5}$$

where a, d, and t are relevant geometric dimensions of SSPP waveguide as shown in Fig. 1a.

The possibility to characterize the state of the electromagnetic field within a single cell with the help of dispersion equation (5) is suggested by the following consideration. In a typical periodically perturbed system, say a photonic crystal, the corresponding band

diagram can be obtained by replicating the dispersion diagram of the background at each reciprocal lattice site. The replicated diagrams intersect at the boundary of the Brillouin zone and the cross-resonance between them leads to opening a gap between the bands. Figure 4(c) shows how the gap formation occurs in a typical photonic crystal. Periodicity thus plays the crucial role for the bandgap formation in a photonic crystal, while far away from the boundary of the Brillouin zone the effect of periodicity on the band is weak.

The bandgap in the spoof plasmon spectrum, however, originates from a different type of mode coupling. The coupling in this case occurs between states inside and outside of the groove and is the strongest at crossing between the light-line and the groove resonant mode at frequency ω_p [see Fig. 4(d)]. It should be emphasized that well-defined SSPP modes are formed when the groove height exceeds half of SSPP period, $h > d/2$,[14] which holds when the intersection between the light-line and the resonant mode is far from the boundary of the Brillouin zone. Thus, in an SSPP supporting structure, periodicity plays rather minor role in the band formation, and one can regard Eq. (5) as describing an effective medium even for a short SSPP structure with minimal number of cells.

Assuming that the interface between the host and defect cells is situated at $x = 0$, the continuity on average condition for the tangential component of the electric field at the interface has the form

$$\int_0^t E_{z(d)}|_{x=0} dz = \int_0^t E_{z(h)}|_{x=0} dz, \tag{6}$$

while the continuity of the total energy flux across the interface leads to

$$\int_0^t E_{z(d)} H^*_{y(d)} dz = \int_0^t E_{z(h)} H^*_{y(h)} dz. \tag{7}$$

Enforcing these conditions, we obtain the transfer matrix for the interface between the host and defect cells

$$\begin{pmatrix} f_{h+} \\ f_{h-} \end{pmatrix} = \frac{1}{2} \begin{pmatrix} t_1 & t_2 \\ t_2 & t_1 \end{pmatrix} \begin{pmatrix} f_{d+} \\ f_{d-} \end{pmatrix} = \widehat{M}_{hd} \begin{pmatrix} f_{d+} \\ f_{d-} \end{pmatrix}.$$

Here $t_j = \frac{1}{2}\left[A - (-1)^j \frac{\beta_d}{\beta_h A} \cdot \frac{2iq_d t}{e^{2iq_d t}-1}\right]$ and $A = i\frac{q_d}{2q_h q_d t}\left(1 - e^{2iq_d t}\right)\frac{1-e^{iq_h t}}{1-e^{iq_d t}}$. For small t, one has $A \approx 1$ and consequently, $t_j \approx \frac{1}{2}\left[1 - (-1)^j \frac{\beta_d}{\beta_h}\right]$. Here q_d and q_h are transverse wavevectors of the defect and host cells, respectively.

An SSPP structure with a defect cell in the middle is described by the transfer matrix

$$\widehat{M} = \widehat{M}_{eh}\widehat{M}_h\widehat{M}_{hd}\widehat{M}_d\widehat{M}_{dh}\widehat{M}_h\widehat{M}_{he}, \tag{8}$$

where $\widehat{M}_{dh} = \widehat{M}_{hd}^{-1}$, $\widehat{M}_{h,d} = \mathrm{diag}\left(e^{i\theta_{h,d}}, e^{-i\theta_{h,d}}\right)$, with $\theta_{h,d} = \beta_{h,d}d$, are the transfer matrices through the host and defect cells, and $\widehat{M}_{eh} = \widehat{M}_{he}^{-1}$ are the transfer matrices between the SSPP structure and environment, which we will take in the form of an interface transfer matrix

$$\widehat{M}_{eh} = \frac{1}{2}\begin{pmatrix} s_1 & -s_2 \\ -s_2 & s_1 \end{pmatrix}, \tag{9}$$

where parameters $s_{1,2}$ can be found using the same continuity-on-average conditions, Eqs. (6) and (7), for the interface between the SSPP structure and environment. Assuming that the incoming wave is characterized by the wavevector $\mathbf{k} = (k_x, 0, k_z)$ with $ck = \omega$, we find $s_j = \frac{1}{2}\left[A' - (-1)^j \frac{2ik_x}{A'\beta} \cdot \frac{q_h t}{1-e^{2iq_h t}}\right]$, where $A' = \frac{q_h k_x}{\beta k_z} \cdot \frac{1-e^{iq_h t}}{1-e^{ik_z t}}$. It should be noted, however, that the specific form of s_j is of low importance for the following.

Since we are interested in the frequency range inside the bandgap of the host structure, where $\beta_h = i\kappa_h$, we present $\theta_h = iNd\kappa_h$, where N is the number of host cells on either side of the defect cell; and obtain from Eq. (8) the transmission coefficient

$$T = -\frac{16e^{i\theta_d}s_1 s_2 t_1 t_2}{e^{2\kappa_h N}\mathcal{D}^{(+)} + e^{-2\kappa_h N}\mathcal{D}^{(-)} + \mathcal{D}^{(0)}}, \tag{10}$$

where

$$\begin{aligned} \mathcal{D}^{(\pm)} &= (s_1 \mp s_2)^2\left[(t_1 \pm t_2)^2 - e^{2i\theta_d}(t_1 \mp t_2)^2\right], \\ \mathcal{D}^{(0)} &= 2(1 - e^{2i\theta_d})\left(s_1^2 - s_2^2\right)\left(t_1^2 - t_2^2\right). \end{aligned} \tag{11}$$

The resonant tunneling occurs at frequency, where the exponential attenuation of the transmission with the length of the host cancels. This yields

$$\mathcal{D}^{(+)}(\omega) = D_+(\omega)D_-(\omega) = 0, \tag{12}$$

where $D_\pm(\omega) = t_1 e^{-i\theta_d/2} \pm t_2 e^{i\theta_d/2}$. Using the obtained transfer matrices, it can be shown that $D_+(\omega) = 0$ and $D_-(\omega) = 0$ define frequencies of states confined to the defect cell embedded into an infinite host structure, even and odd with respect to the center of the defect cell, respectively. It's not difficult to see, however, that $D_+(\omega) = 0$ does not have solutions inside the first Brillouin zone. Thus, the resonant transmission is supported only by odd local states, or when

$$\frac{\beta_d(\omega)}{\kappa_h(\omega)} = \cot\left(\frac{d\beta_d(\omega)}{2}\right). \tag{13}$$

Basic features of the transmission resonance can be discussed directly on the base of Eq. (13) taking into account that inside the bandgap above host spoof plasma frequency ω_h, (i.e., $\omega_h < \omega < \omega_h^{(H)}$), we have

$$\kappa_h = \frac{\omega}{c}\sqrt{\frac{\omega_h^{(H)} - \omega}{\omega - \omega_h}}. \tag{14}$$

Here, $\omega_h^{(H)}$ is the upper frequency edge of the SSPP bandgap, which is found to be

$$\omega_h^{(H)} = \omega_h \left(1 + \frac{4ah}{\pi^2 dt}\right). \tag{15}$$

One can see that, for example, as the height of the groove of the defect cell increases, the transmission resonance ω_r emerges near $\omega_h^{(H)}$ and moves deeper into the host bandgap ($\omega_h^{(H)} - \omega_r \sim \sqrt{h_d - h_h}$). The comparison between the analytical estimation of characteristic resonant frequencies (ω_r) following from Eq. (13) and the numerical results is provided in Fig. 2(d). The good agreement of our analysis with the numerically obtained data validates the concept that spoof plasmon mode can survive even in a short meta-structure consisting of minimal number of cells. It should be noted that when the resonance frequency ω_r approaches ω_h, the point $\beta_d(\omega_r)$ gets close to π/d, where the characterization of the state of the electromagnetic field inside the defect cell in terms of dispersion equation (5) is no longer valid and Eq. (13) breaks down.

We conclude this section with a note about the defect induced anti-resonances in transmission spectra, for instance, at $\omega/\omega_h \approx 1.45$ in Fig. 2(b) and at $\omega/\omega_h \approx 0.7$ and 2.2 in Fig. 2(c). They, as well, can be studied using Eq. (10). It's not difficult to see that they emerge at frequencies inside the stop-band of the defect cell. As a result, with the variation h_d, they follow defect cell spoof plasma frequencies, $\omega_d^{(n)}$.

IV. Q-FACTOR AND ENHANCED RADIATION RATE

We consider two figures of merit for the resonant mode inside the SSPP bandgap: the Q-factor and the Purcell factor. In a defect incorporated finite waveguide, for a given frequency inside the bandgap, the fraction of power transmitted through the structure can be written as

$$|T|^2 \sim e^{-4\kappa_h dN}. \tag{16}$$

As the Q-factor is inversely proportional to the power radiated out of the structure, taking into account Eq. (14) for κ_h, we can estimate it for frequencies not too close to ω_p as

$$\log Q \sim N\sqrt{\frac{\omega_h^{(H)} - \omega_r}{\omega_r - \omega_h}}. \tag{17}$$

As has been discussed above, with the gradual change of the height of the groove in the defect cell, the resonance frequency approaches ω_h, which results in significant increase of κ_h, yielding very high quality modes localized on the defect cell.

Figure 5a shows how the quality factor changes with the variation of the defect's spoof plasma frequency. The fact that electromagnetic transmission essentially stops at ω_h results in exponential increase of the Q-factor. Thus, a very high quality resonating mode is possible to realize in an SSPP host medium consisting of only one groove on each side of the defect cell. Although the divergence in Eq. (17) is an artifact of the approximation retaining only single mode inside the grooves, the COMSOL Multiphysics full-wave simulation justifies very high Q-factor in the (1–1–1) structure, which hits a maximum of value of 10^5 when resonant mode frequency coincides with the host spoof plasma frequency ω_h.

The high quality resonant mode formed by the simple SSPP structure signifies strong field localization near the defect cell at the sub-wavelength scale. This inspires us to investigate the Purcell effect, F_P, which is the modification of the spontaneous decay rate of source when it matches to the resonant mode of a cavity. In plasmonics, this effect is related to a large local-field enhancement in 'hot spots' due to the creation of surface plasmons, which can be manipulated to build coherent light sources with ultra-low lasing threshold[40]. For a good quality cavity with low loss and quasi-normal eigenmodes, the magnitude of the decay rate enhancement can be estimated using[41]

$$F_P = \frac{3}{4\pi^2}\frac{(\lambda_c/n)^3}{V}Q, \tag{18}$$

where λ_c/n is the wavelength within the material and V is the mode volume. Near the spoof plasma frequency of the host, the volume occupied by the resonant mode can be estimated as 2×(volume of host groove) + (volume of defect cell). For the (1–1–1) heterostructure with 100 μm groove width and 800 μm height, we obtain $\lambda_c^3/V \approx 16$ near 0.1 THz. Thus, on top of enhanced radiation rate of emitter contributed by high Q-factor of cavity, we expect at least an extra order of increment of Q/V ratio solely contributed by the mode volume reduction of defect incorporated SSPP structure.

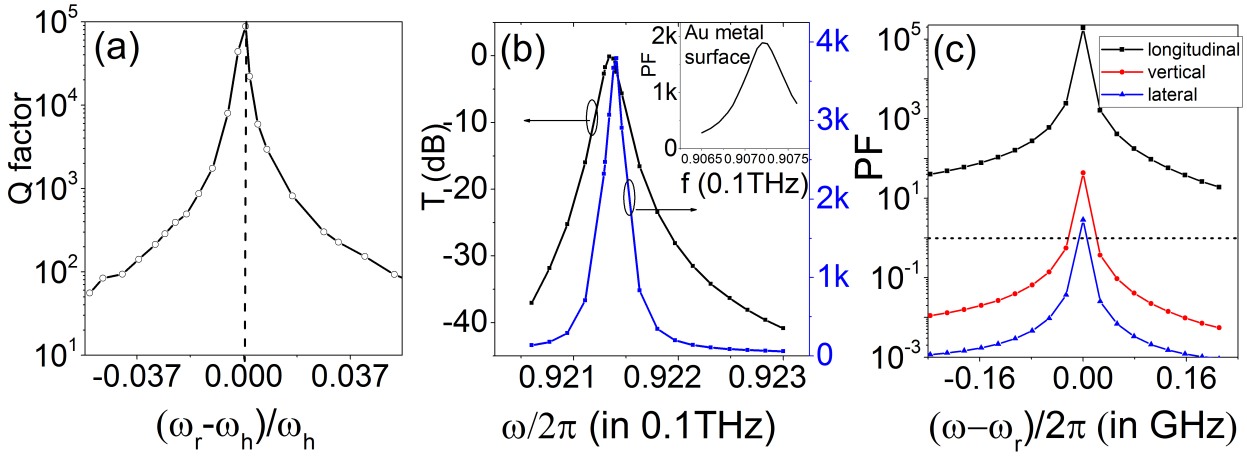

FIG. 5. (a) The Q-factor as a function of the difference between the frequency of resonant tunneling and host's spoof plasma frequency. The height of each grooves = 0.8 mm, period = 1 mm, arm = 300 μm, defect's optical height = 2.5mm. (b) The Purcell factor, F_P, in the limit of perfect electric conductor in the (1–1–1) heterostructure is plotted together with the transmission spectrum. Inset shows the Purcell factor around the resonant frequency for a structure of the same geometry but with Au metal surface. (c) The frequency dependence of the Purcell factor for sources with three different dipole orientations, positioned near the groove opening in the defect cell. The region above the dotted line corresponds to $F_P > 1$.

In order to confirm large values of the Purcell factor obtained from this estimate, we numerically evaluate the total power emission by a point dipole source placed inside a heterogeneous (1–1–1) SSPP structure. A practical implementation for the point dipole source in the relevant frequency range can be n-doped GaAs based submicron size Gunn oscillator, which can operate in the lower part of THz range[42]. More importantly, its miniature physical size justifies the 'point' sized source assumption, so as not to alter the photonic density of states of the meta-material.

As the waveguide has a metallic cover at distance t away from the groove, the only gateway for power outflow from a source placed inside the waveguide is the lateral opening of the waveguide at each terminal. The magnitude of the source is set in such a way so that it irradiates unity magnitude power when placed in free space.

The total power radiated by a Hertzian dipole radiated over all direction is

$$P_{air} = \int_0^{2\pi} d\phi \int_0^{\pi} d\theta \langle S_r \rangle r^2 sin\theta = \frac{\eta_0}{12\pi}(k\bar{I}d)^2. \tag{19}$$

For a given frequency ω, a dipole current source $\bar{I}d(\omega)$ is chosen so as to emit $P_{air} = 1$ unit. In our 3D simulations, we take the lateral dimension, w, of the waveguide to satisfy $w \gg d$, so that the boundary condition along the lateral direction does not have significant impact on the overall system. When the defect cell is excited with its resonant mode, a large field density occurs on top of the defect groove-mouth. Since the resonant mode is predominant with the longitudinal E_x component, the polarization direction of the dipole source is chosen as x-axis.

Figure 5(b) shows the Purcell factor spectrum around the frequency of the resonant tunneling mode. The maximum of the Purcell factor coincides with the frequency of maximal transmission. With the Q-factor reaching the value $\sim 1.5 \times 10^2$ at the resonant frequency, the radiation enhances by a factor of 4×10^3. The inset of Fig. 5(b) shows Purcell factor for the structure of the same geometry but instead of the perfect electric conductor we have chosen material with the conductivity of gold at 0.1 THz. While retaining large values, both the quality factor and the peak transmission are reduced due to the finite conductivity, especially near the host plasma frequency. A detailed account of the effect of the trade-off between the mode confinement and the Q-factor in heterogeneous SSPP structure in the presence of finite conductivity will be provided elsewhere.

We have extended our analysis of the Purcell factor enhancement for dipole sources with different orientations [Fig. 5(c)]. As expected, the largest contribution to radiation enhancement appears from the longitudinal component of the dipole moment of the source, since the propagating SSPP mode with the lowest frequency is predominantly E_x polarized field. This is why, the x-polarized dipole source emits many orders of magnitude larger power than that polarized in other directions. This in turn implies that, even for a source with a random orientation of dipole moment, the maximum oscillation strength would reduce just by a factor of three.

V. CONCLUSION

We have shown that, opposed to commonly held view, realization of an ultrahigh quality resonant SSPP mode with enhanced emissivity does not require a large host medium to admit well developed defect modes. Even within a single cell, the electromagnetic states can be described with a good accuracy by the SSPP dispersion law obtained for a periodic

structure. This is attributed to the fact that the spoof plasmon mode originates from coupling between propagating free-space modes and the groove resonances within each cell, rather than from the cell-to-cell coupling.

The formation of SSPP modes well defined even in structures with small number of cells allows designing a tunable SSPP composite system made of one host cell on each side of a defect cell. Coupling between the SSPP states in the defect cell and in the host leads to formation of a narrow transmission resonance inside the bandgap of the host structure. We show that the Q-factor of the defect state can easily reach the value of 10^5 together with the large spontaneous radiation rate (exceeding 10^3). Both the Q-factor and the Purcell factor reach their maximum values when the optical height of the groove in the defect cell is tuned to yield the transmission resonance near the spoof plasma frequency of the host structure.

Reducing the size of the entire defect-host system to the minimum possible value is quintessential for making ultra-compact sources, especially at micro-wave and low terahertz region. The same principle may also be extended to higher frequencies and using highly doped semiconductor instead of metal, though keeping in mind that the Ohmic losses in real metal/material due to longer relaxation time of electron's response would begin competing with the long-lived resonating mode. Nevertheless, the redundancy of periodicity in spoof plasmonic waveguides together with strong lateral confinement in a specified spectral zone, we believe, presents great opportunities for expedition of the emerging field of spoof-plasmon science.

ACKNOWLEDGEMENT

This work was supported in part by the Air Force Office of Scientific Research under Grant FA 9550-12-1-0402 and in part by the National Science Foundation under Grant 1116040.

---

* srjoy@umich.edu

† merement@umich.edu

‡ pinakimazum@gmail.com

[1] J. Pendry, L. Martin-Moreno, and F. Garcia-Vidal, Science **305**, 847 (2004).

[2] X. Shen, T. J. Cui, D. Martin-Cano, and F. J. Garcia-Vidal, Proc. Nat. Acad. Sci. **110**, 40 (2013).

[3] N. Yu, Q. J. Wang, M. A. Kats, J. A. Fan, S. P. Khanna, L. Li, A. G. Davies, E. H. Linfield, and F. Capasso, Nature Mater. **9**, 730 (2010).

[4] S. A. Maier, S. R. Andrews, L. Martin-Moreno, and F. Garcia-Vidal, Phys. Rev. Lett. **97**, 176805 (2006).

[5] J. Yang, C. Sauvan, H. Liu, and P. Lalanne, Phys. Rev. Lett. **107**, 043903 (2011).

[6] A. Rusina, M. Durach, and M. I. Stockman, Appl. Phys. A **100**, 375 (2010).

[7] J. Wood, L. Tomlinson, O. Hess, S. Maier, and A. Fernández-Domínguez, Phys. Rev. B **85**, 075441 (2012).

[8] K. Song and P. Mazumder, IEEE Trans. Electron Dev. **56**, 2792 (2009).

[9] A. Pors, E. Moreno, L. Martin-Moreno, J. B. Pendry, and F. J. Garcia-Vidal, Phys. Rev. Lett. **108**, 223905 (2012).

[10] Z. Liao, Y. Luo, A. I. Fernández-Domínguez, X. Shen, S. A. Maier, and T. J. Cui, Sci. Rep. **5** (2015).

[11] X. Shen and T. J. Cui, Laser Photonics Rev. **8**, 137 (2014).

[12] R. Stanley, Nature Photon. **6**, 409 (2012).

[13] F. Garcia-Vidal, L. Martin-Moreno, and J. Pendry, J. Opt. A: Pure Appl. Opt. **7**, S97 (2005).

[14] M. Erementchouk, S. R. Joy, and P. Mazumder, *Proc. R. Soc. A*, **472**, 20160616 (2016).

[15] M. A. Kats, D. Woolf, R. Blanchard, N. Yu, and F. Capasso, Opt. Express **19**, 14860 (2011).

[16] C. Wu, A. Salandrino, X. Ni, and X. Zhang, Phys. Rev. X **4**, 021015 (2014).

[17] S. Noda, K. Tomoda, N. Yamamoto, and A. Chutinan, Science **289**, 604 (2000).

[18] W. Cai and V. M. Shalaev, *Optical metamaterials*, Vol. 10 (Springer, 2010).

[19] N. Engheta and R. W. Ziolkowski, *Metamaterials: physics and engineering explorations* (John Wiley & Sons, 2006).

[20] E. Yablonovitch, J. Opt. Soc. Am. B **10**, 283 (1993).

[21] Y.-J. Lu, J. Kim, H.-Y. Chen, C. Wu, N. Dabidian, C. E. Sanders, C.-Y. Wang, M.-Y. Lu, B.-H. Li, X. Qiu, *et al.*, Science **337**, 450 (2012).

[22] S. Wu, S. Buckley, J. R. Schaibley, L. Feng, J. Yan, D. G. Mandrus, F. Hatami, W. Yao, J. Vučković, A. Majumdar, *et al.*, Nature **520**, 69 (2015).

[23] J. N. Anker, W. P. Hall, O. Lyandres, N. C. Shah, J. Zhao, and R. P. Van Duyne, Nature Mater. **7**, 442 (2008).

[24] A. Wallraff, D. I. Schuster, A. Blais, L. Frunzio, R.-S. Huang, J. Majer, S. Kumar, S. M. Girvin, and R. J. Schoelkopf, Nature **431**, 162 (2004).

[25] A. Akimov, A. Mukherjee, C. Yu, D. Chang, A. Zibrov, P. Hemmer, H. Park, and M. Lukin, Nature **450**, 402 (2007).

[26] S. Han, Y. Xiong, D. Genov, Z. Liu, G. Bartal, and X. Zhang, Nano Lett. **8**, 4243 (2008).

[27] D. R. Smith, J. B. Pendry, and M. C. Wiltshire, Science **305**, 788 (2004).

[28] M. Minkov and V. Savona, Sci. Rep. **4**, 5124 (2014).

[29] X. Gan, R.-J. Shiue, Y. Gao, K. F. Mak, X. Yao, L. Li, A. Szep, D. Walker Jr, J. Hone, T. F. Heinz, *et al.*, Nano Lett. **13**, 691 (2013).

[30] F. Lemoult, N. Kaina, M. Fink, and G. Lerosey, Nature Phys. **9**, 55 (2013).

[31] N. Kaina, F. Lemoult, M. Fink, and G. Lerosey, Appl. Phys. Lett. **102**, 144104 (2013).

[32] K. Ho, C. T. Chan, and C. M. Soukoulis, Phys. Rev. Lett. **65**, 3152 (1990).

[33] J. D. Joannopoulos, P. R. Villeneuve, S. Fan, *et al.*, Nature **386**, 143 (1997).

[34] V. Astratov, D. Whittaker, I. Culshaw, R. Stevenson, M. Skolnick, T. Krauss, and R. De La Rue, Phys. Rev. B **60**, R16255 (1999).

[35] W. L. Barnes, A. Dereux, and T. W. Ebbesen, Nature **424**, 824 (2003).

[36] X.-S. Lin and X.-G. Huang, Opt. Lett. **33**, 2874 (2008).

[37] Z. Li, J. Xu, C. Chen, Y. Sun, B. Xu, L. Liu, and C. Gu, Appl. Opt. **55**, 10323 (2016).

[38] S. Fan, Appl. Phys. Lett. **80**, 908 (2002).

[39] Z. Xu, K. Song, and P. Mazumder, IEEE Trans. Terahertz Sci. Technol. **2**, 345 (2012).

[40] W. Wei, X. Yan, and X. Zhang, Sci. Rep. **6** (2016).

[41] E. M. Purcell, Phys. Rev. **69**, 681 (1946).

[42] F. Amir, C. Mitchell, N. Farrington, and M. Missous, in *SPIE Europe Security+ Defence* (International Society for Optics and Photonics, 2009) pp. 74850I–74850I.